Nano-encapsulation of a novel anti-Ran-GTPase peptide for blockade of regulator of chromosome condensation 1 (RCC1) function in MDA-MB-231 breast cancer cells

*Graphical Abstract (for review)

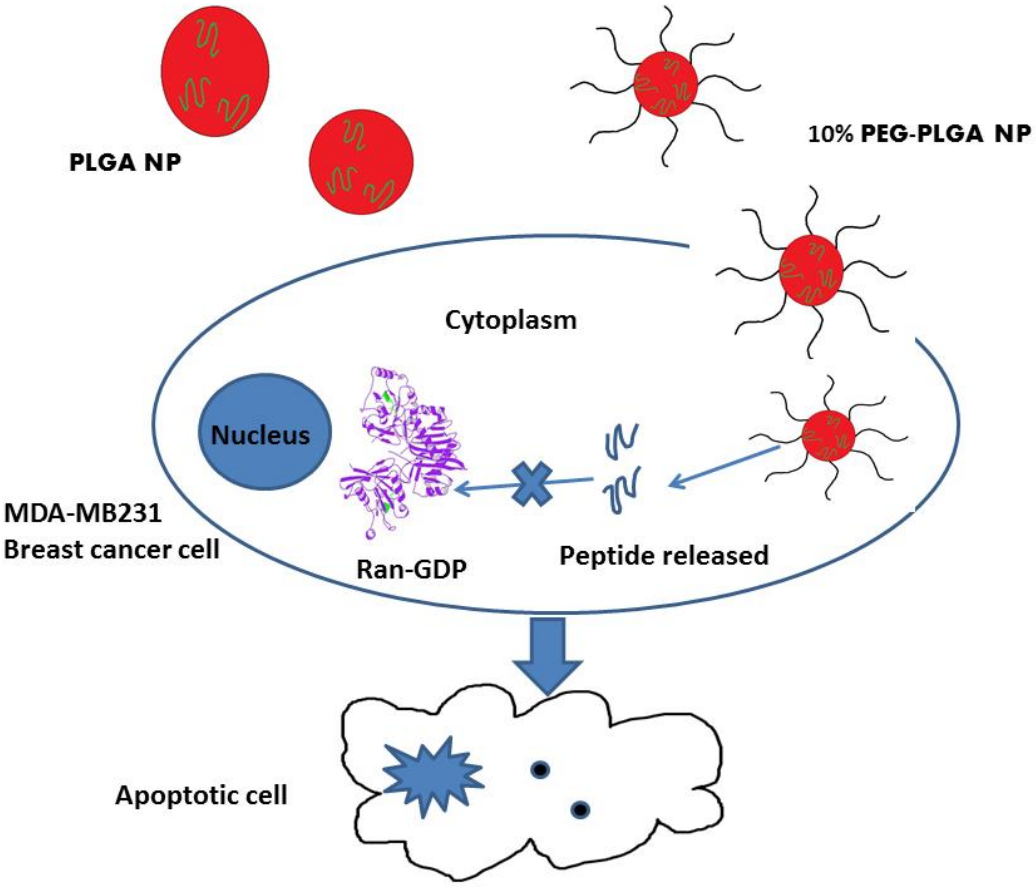

Nano-encapsulation of a novel anti-Ran-GTPase peptide for blockade of regulator of chromosome condensation 1 (RCC1) function in MDA-MB-231 breast cancer cells

Yusuf A. Haggag [a,b], Kyle B. Matchett [c], Dakir El-Habib [c,d], Paul Buchanan [c], , Mohammed A. Osman [b], Sanaa A. Elgizawy [b], Mohamed El-Tanani [c,d,f] , Ahmed M. Faheem [b,e,1], Paul A. McCarron [a,1,*]

[a] School of Pharmacy and Pharmaceutical Sciences, Saad Centre for Pharmacy and Diabetes, Ulster University, Cromore Road, Coleraine, Co. Londonderry, BT52 1SA, UK.

[b] Department of Pharmaceutical Technology, Faculty of Pharmacy, University of Tanta, Tanta, Egypt.

[c] Centre for Cancer Research and Cell Biology, Queen's University Belfast, Belfast BT9 7BL, UK.

[d] Institute of Cancer Therapeutics, University of Bradford, Bradford, UK.

[e] Sunderland Pharmacy School, Department of Pharmacy, Health and Well Being, University of Sunderland, Sunderland SR1 3SD.

[f] IDT (Imhotep Diagnostics and Therapeutics), Europa Tool House, Springbank, Industrial Estate, Dunmurry, Northern Ireland.

[1]Both authors contributed equally to the work

*Corresponding author
Paul A. McCarron
School of Pharmacy and Pharmaceutical Sciences,
Ulster University,
Cromore Road,
Coleraine,
Co. Londonderry,
BT52 1SA, UK
Tel: +44 (0) 28 70124284
Fax: +44 (0) 28 70123518
Email: p.mccarron@ulster.ac.uk

Abstract

Ran is a small ras-related GTPase and is highly expressed in aggressive breast carcinoma. Overexpression induces malignant transformation and drives metastatic growth. We have designed a novel series of anti-Ran-GTPase peptides, which prevents Ran hydrolysis and activation, and although they display effectiveness *in silico*, peptide activity is suboptimal *in vitro* due to reduced bioavailability and poor delivery. To overcome this drawback, we delivered an anti-Ran-GTPase peptide using encapsulation in PLGA-based nanoparticles (NP). Formulation variables within a double emulsion solvent evaporation technique were controlled to optimise physicochemical properties. NP were spherical and negatively charged with a mean diameter of 182–277 nm. Peptide integrity and stability were maintained after encapsulation and release kinetics followed a sustained profile. We were interested in the relationship between cellular uptake and poly(ethylene glycol) (PEG) in the NP matrix, with results showing enhanced *in vitro* uptake with increasing PEG content. Peptide-loaded, pegylated (10% PEG)-PLGA NP induced significant cytotoxic and apoptotic effects in MDA-MB-231 breast cancer cells, with no evidence of similar effects in cells pulsed with free peptide. Western blot analysis showed that encapsulated peptide interfered with the proposed signal transduction pathway of the Ran gene. Our novel blockade peptide prevented Ran activation by blockage of regulator of chromosome condensation 1 (RCC1) following peptide release directly in the cytoplasm once endocytosis of the peptide-loaded nanoparticle has occurred. RCC1 blockage was effective only when a nanoparticulate delivery approach was adopted.

Keywords

Anti-Ran-GTPase peptide, double emulsion, PLGA, nanoparticle, breast cancer, drug delivery.

1. Introduction

Nanotechnologies offer promising approaches for the diagnosis and treatment of neoplastic disease, which remains a major on-going public health concern (Sharma et al., 2013). Effective delivery of the therapeutic agent often poses challenges, especially if it is peptide in nature and its site of action is inaccessible. Furthermore, tumour metastasis is a predominant feature in many cancer-related deaths (Palmer et al., 2011), making complete disease remission and cure more difficult. Therefore, an awareness and understanding of target pathways is essential to the development of novel therapeutics. Specifically, recent studies show that Ran (Ras-related nuclear) protein is involved in growth regulation, apoptotic resistance, tumour transformation, increased aggressiveness and enhanced metastasis in a wide range of tumour types, such as breast, and is, therefore, a potential therapeutic target (Abe et al., 2008; Kurisetty et al., 2008; Ly et al., 2010; Xia et al., 2008; Yuen et al., 2012).

Ran is a member of the Ras superfamily that regulates nucleocytoplasmic transport, mitotic spindle fibre assembly and post-mitotic nuclear envelope dynamics (Matchett et al., 2014). Ran acts as a molecular switch through a GTP-GDP cycle (Rush et al., 1996; Sazer, 1996) in which the conversion between GTP-bound and GDP-bound conformations controls its interaction with different effectors (Scheffzek et al., 1995; Vetter et al., 1999). Ran-GTP is formed inside the nucleus by interaction of Ran with its specific guanine nucleotide exchange factor (GEF), termed RCC1, which catalyses the exchange of GDP for GTP (and *vice versa*) on the nucleotide binding pocket of Ran (Bischoff and Ponstingl, 1991a; Bischoff and Ponstingl, 1991b; Ohtsubo et al., 1989; Renault et al., 2001). Our group have shown that the interaction between Ran-GDP and RCC1 can be disrupted using different novel blockade peptides that inhibit competitively the binding of RCC1 to its specific binding pocket in the Ran-GDP conformation.

In order to block Ran-GDP-dependent RCC1 function, our group have identified segments of the Ran protein sequence that are predicted to interact with RCC1 in the formation or stabilisation of the Ran-GDP-RCC1 complex. We have designed a family of synthetic peptides designed to be biologically active, comprising a contiguous sequence of at least 6 amino acids and extending up to 25 amino acids (Patent Application GB1607593.9). *In silico* design enabled our group to deliver a predictable method for the generation of peptide inhibitors of the Ran-RCC1 interaction that are fragments of the natural Ran protein. However, our preliminary data have demonstrated that delivery of these anticancer therapeutic peptides to deep subcellular sites of action remains a substantial challenge due to poor cellular distribution, lack of selective delivery and multidrug resistance. These findings are shared with the delivery of many other therapeutic peptides (Brigger et al., 2002).

The development of peptide-based therapeutics has had promising results (Thayer, 2011), both in terms of efficacy and targeting specificity (Aina et al., 2002; Enbäck and Laakkonen, 2007; Vlieghe et al., 2010). Biodegradable polyester matrices, in particular, feature in many innovative approaches evaluated over the past four decades. Formulations based on PLGA matrices have secured FDA approval in the treatment of advanced prostate and breast cancers (West et al., 1987). Similarly, FDA approval is in place for other peptide drugs incorporated within polymeric carriers, such as leuprolide acetate indicated for the treatment of advanced prostate and breast cancers (Sethi and Sanfilippo, 2009), and a controlled release formulation based on octreotide acetate-loaded PLGA for tumour treatment in neuroendocrine disorders and carcinoid syndrome (Anthony and Freda, 2009). A PLGA-based microparticle formulation of triptorelin pamoate used for advanced prostate cancer and other indications, was given regulatory approval in 2000 (Crawford and Phillips, 2011). However, the formidable barrier to effective peptide transport across the cell membrane remains. Lipid-based nanocarriers and colloidal nanoparticles (NP) are often used to

encapsulate biologically active drugs, such as peptides, proteins and DNA, and to enhance cell penetration (Angelov et al., 2012; Angelova et al., 2013a; Angelova et al., 2013b; Angelova et al., 2015; Angelova et al., 2011; Borghouts et al., 2005). Polymeric NP made from poly(lactic-*co*-glycolic acid) (PLGA) are especially beneficial (Haggag and Faheem, 2015; Kamaly et al., 2012).

PLGA NP are fabricated using a range of techniques (Jain, 2000), with the emulsion-solvent evaporation technique frequently used to encapsulate small molecular weight compounds, like peptides, and high molecular weight DNA or antisense oligonuclotides (Labhasetwar, 1997). Given the unique nature of our novel anti-Ran-GTPase blockade peptide, the first aim was to adjust formulation parameters in a emulsion-solvent evaporation technique, such as the PEG fraction in the polymer matrix, peptide loading and volume of external aqueous phase. This would evaluate, for the first time, how the presence of our peptide would affect properties, such as mean particulate size and its distribution. The second aim was to maximise the encapsulation efficiency of our peptide, designed specifically to interact with and deactivate Ran-GTP, and assess stability and release. The third aim of the work was to investigate the effectiveness of cellular uptake and evaluate interaction between the blockade peptide and the Ran gene in a breast cancer cell line (MDA-MB-231), which is characterised by Ran overexpression.

2. Materials and Methods

2.1 Materials

PLGA with a 50:50 lactic:glycolic ratio (Resomer® RG 503H, MW 34 kDa) and two PLGA-co-PEG block copolymers (Resomer® RGP d 5055 (5% PEG of MW 5 kDa) and Resomer® RGP d 50105 (10% PEG of 5 kDa molecular weight)) were purchased from Sigma Chemical Co. (St. Louis, USA). An anti-Ran-GTPase blockade peptide (CAQGEPQVQFK, composed

of 11 amino acids with a molecular formula of $C_{53}H_{83}N_{15}O_{17}S$, a purity of ≥ 94%, molecular weight 1234 Da, and estimated good water solubility) was synthesised by GL-Biochem Ltd. (Shanghai, China). Poly(vinyl alcohol) (PVA, 87-89% hydrolysed, molecular weight 31,000-50,000) and phosphate-buffered saline (PBS) were obtained from Sigma Chemical Co. (St. Louis, USA). A modified Lowry Protein Assay kit was obtained from Pierce Ltd. (Rockford, IL). Dichloromethane, acetonitrile and triflouroacetic acid were of HPLC grade and other reagents were of analytical grade. Water used in the work was produced to Type 1 standard (Milli-Q®, 18.2 MΩ cm at 25 °C).

MDA-MB-231 breast cancer cells were obtained from Prof. Mohamed El-Tanani (Institute of Cancer Therapeutics, Bradford University) and grown in Dulbecco's modified Eagle's medium (DMEM) supplemented with 10% (v/v) foetal bovine serum (FBS), 2 mmol l^{-1} L-glutamine, 100 U ml^{-1} of penicillin and 100 μg ml^{-1} streptomycin (Invitrogen, Carlsbad, CA, USA) at 37 ºC in humidified 95% air and 5% CO_2 with medium changed after each three-day interval.

2.2 Preparation of peptide-loaded NP

A modified, double emulsion, solvent evaporation method (Haggag et al., 2016) was used in this study. Anti-Ran-GTPase blockade peptide was dissolved in 0.2 ml of internal aqueous phase (Table 1) and mixed with 2.0 ml dichloromethane (DCM) containing 5% w/v polymer, then emulsified at 6,000 rpm (Silverson L5T, Silverson Machines, UK) for 2 minutes. The primary emulsion (w/o) was injected directly into a 1.25% w/v PVA solution under agitation and emulsification continued at 10,000 rpm for a further 6 minutes to produce a double emulsion, using the same conditions of homogenisation. The final emulsion was stirred by magnetic agitation overnight under vacuum to evaporate the organic solvent. After the nanospheres had formed, they were centrifuged at 22,000 *g* for 30 minutes at 4 °C, which was

sufficient to pellet the NP. The pellet was washed three times with ultrapure water, washed once with 2% w/v sucrose solution and lyophilised (Labconco, Kansas city, Missouri). Samples were stored in a desiccator at ambient temperature before further use.

To make fluorescent peptide-loaded NP, coumarin 6 (100 µg) was added to the DCM phase, as the only change to the procedure described above. NP containing coumarin 6 were evaluated with respect to the drug-loading efficiency, particle size, polydispersity index (PDI) and zeta potential. Process variables, such as the PEG content, peptide loading, volume of external aqueous phase and composition of the internal aqueous phase are listed in Table 1, together with the identifying code used to define each NP formulation.

2.3 NP Characterisation

Lyophilised NP samples (5.0 mg) were suspended in Milli-Q water to a suitable concentration to give the recommended scattering intensity of 100,000 counts per second. The mean diameter and size distribution were analysed by photon correlation spectroscopy (PCS) at a fixed angle of 90° using a Malvern Zetasizer 5000 (Malvern Instruments, UK). All measurements were performed in triplicate. Surface charge was quantified as zeta potential using laser Doppler anemometry (Malvern Zetasizer 5000, Malvern Instruments, UK). Lyophilised samples were diluted with 0.001 M KCl. Zeta potentials were calculated from the mean value of electrophoretic mobility by applying the Smoluchowski equation. All measurements were performed in triplicate. NP surface morphology was studied using scanning electron microscopy (FEI Quanta 400 FEG SEM). Powder samples were mounted on to metal stubs, then coated with a gold layer under vacuum before scanning.

2.4 Determination of peptide loading, encapsulation efficiency and concentration

Peptide loading was determined by direct extraction from lyophilised NP following common solvent dissolution using dimethylsulfoxide (DMSO). Freeze-dried NP (10 mg) were weighed accurately, dissolved in 1.0 ml DMSO and added to a solution of 0.1 N NaOH containing 0.5% SDS. After standing for 1 hour at room temperature, the suspension became transparent. The peptide concentration was measured by the Lowry method (Fude et al., 2005), giving the percentage loading (w/w, peptide mass per unit mass of dry NP). Comparison of the actual peptide loading with the theoretical peptide loading gave the percentage encapsulation efficiency. Each sample was assayed in triplicate.

The concentration of free peptide obtained during release studies was determined using HPLC. Reverse phase chromatography (Alcock et al., 2002) (Phenomenex- Luna® C18-5 column mm, 5 µm) running at a flow rate of 1.0 ml min^{-1} with UV detection (254 nm) was used. A mobile phase elution gradient was established, comprising two solvent mixtures (solvent A 0.1% TFA in acetonitrile; solvent B 0.1% TFA in water).

2.5 In vitro release studies

A sample of peptide-loaded NP (5.0 mg) was suspended in 1.0 ml PBS (pH 7.4) solution and incubated at 37 °C with agitation using a reciprocal shaking water bath (100 rpm). Samples were taken at predetermined time intervals of 1, 12, 24, 48, 72, 96, 120, 144 and 168 hours, replaced with fresh PBS, centrifuged for 5 minutes at 22,000 *g* and the peptide concentration in the supernatant determined in triplicate by HPLC assay.

2.6 Assessment of peptide integrity

The stability of encapsulated peptide following formulation and release from polymeric NP was determined after 7 days of *in vitro* release. The aqueous release medium containing

peptide was analysed immediately using HPLC-MS (Applied Biosystems API 4000 LC/MS/MS). The mobile phase, at a flow rate of 1.0 ml min^{-1}, comprised a linear gradient of solvent B (0.1% TFA in acetonitrile) in solvent A (0.1% TFA in water) over a run time of 30 minutes. About 10–20 µl of the sample was separated using a C18 reversed phase column. The XCALIBUR® software package (Thermo scientific, USA) was used for data acquisition and analysis.

2.7 Seeding of MDA-MB-231 cells

MDA-MB-231 cells were harvested, once confluent, and the suspension centrifuged at 1200 rpm (4 °C) for 5 minutes to sediment the cells. The pellet was re-suspended in complete growth medium (DMEM (high glucose), 10% fetal bovine serum (FBS), 0.1 mM MEM Non-Essential Amino Acids (NEAA), 2 mM L-glutamine, 1% Pen-Strep). A cell count was performed on a sample of suspension (10 µl) using a haemocytometer.

2.8 Cellular uptake of NP

Cellular uptake of coumarin 6-loaded NP formulations was evaluated using flow cytometry and fluorescence microscopy (Pamujula et al., 2012). Briefly, 1.5×10^5 MDA-MB31 cells were seeded onto 6-well tissue culture plates in 2.0 ml complete growth medium one day before the experiment. For FACS analysis, coumarin 6-tagged NP (F16, 17 and F18) were suspended in Optimem® media and added to MDA-MB-231 cells for 24 hours in 6-well plates. Cells were removed by trypsinisation and resuspended in FACS buffer. Cellular uptake of NP was quantified by gating for positive couramin 6 staining in the FITC channel following control staining with coumarin 6-treated and unstained MDA-MB-231 cells. Three independent experiments with three replicates were performed for each assay.

Cellular uptake and cellular localisation of the peptide-loaded NP were evaluated qualitatively by fluorescence microscopy using analysis of five fields per well. Intracellular uptake of coumarin 6-loaded NP (F18) into MDA-MB-231 cells was detected using fluorescence imaging 24 hours after treatment (Olympus IX70). The images were captured using digital photography (Olympus DP-71, Olympus, Centre Valley, PA, USA). MDA-MB-231 cells where seeded into a 6-well plate, containing two fixed cover slips and 2.0 ml of growth medium. After washing cells with sterile PBS, the coverslips were removed, mounted with fixing media over a glass slide and examined. The untreated MDA-MB-231 cells and cells treated with a solution of coumarin 6 were used as positive and negative controls, respectively.

2.9 Cytotoxicity studies

Cytotoxicity of an optimised peptide-loaded NP formulation (F18) was measured by assessing cell viability (MTT assay). MDA-MB-231 cells were seeded in 24-well plates (Nalgen Nunc International, Ochester, NY) at a density of $5x10^4$ cells suspended in 0.5 ml media per well and incubated for 24 hours to allow for 60-70% confluency and sufficient adhesion. Cells were treated with 1.0 ml of transfection medium containing different concentrations of peptide (2.0 μM, 4.0 μM and 8.0 μM) in either free form or encapsulated in NP. Encapsulation efficiency data was used to determine the required mass of peptide-loaded NP needed to maintain peptide equivalency to the free peptide solutions. As a control experiment, cells were exposed to a concentration of blank NP equivalent to the highest concentration of peptide-loaded NP used.

After 24, 48, 72 and 96 hours, the treated cells were washed with 500 μl PBS and 500 μl of 15% MTT dye solution in complete media. The plates were incubated at 37 °C and 5% CO_2 for an additional 3 hours. The supernatant was discarded and MTT-formazan crystals

formed by metabolically viable cells dissolved in 500 µl of dimethylsulfoxide (DMSO). The optical density of each well was measured at 570 nm (reference wavelength 630 nm) in a microplate reader (Fluostar Omega, BMG Lab Tech GMBH, Germany). This experiment was performed in triplicate and repeated three times. Mean values ± standard deviation (SD) for each concentration were determined. Percentage cell viability was determined as the ratio of absorbance (570 nm) in treated cells relative to the absorbance in control cells (570 nm). The absorbance of the untreated cells was set at 100%. The IC_{50} was defined as the concentration of sample needed to reduce the signal by 50% relative to the control.

2.10 Cell cycle analysis

To determine the effect of peptide-loaded NP on cell growth, cultured cells were treated with the same doses of free peptide and peptide-loaded NP as used in the cell viability assay. MDA-MB31 cells (1.5×10^5) were seeded onto 6-well tissue culture plates in 2 ml complete growth medium one day before the experiment. After 24 and 48 hours of treatment, cells were suspended in PBS and fixed by addition of 70% ice-cold ethanol. Cells were treated by adding RNase (1.0 µg ml^{-1}) to the samples and resuspending in propidium iodide (PI) stain (5.0 µg ml^{-1}). Cellular DNA content was analysed (FACS Calibur, BD Biosciences) using approximately 10,000 cells for each analysis. The distribution of cells in each phase of the cell cycle was displayed in histogram format. Flow-cytometric data were analysed using Cyflogic (v.1.2.1) software. Quantification of apoptotic cells was determined as the percentage of cells in the sub-G1 region (hypodiploidy) in cell cycle analysis, as previously described (Looi et al., 2011). The assay was repeated at least twice and the treatments were tested in duplicate.

2.11 Ran activation assay

MDA-MB31 cells (1.5×10^5) were seeded onto 6-well tissue culture plates in 2.0 ml complete growth medium one day before the experiment commenced. Measurement of Ran activity was captured using a Ran activation assay kit (Yuen et al., 2013) (Cell Biolabs, San Diego, CA) and used according to the manufacturer instructions. This Ran activation assay is used to visualise a Ran-GTP band, which means Ran is in its active form. It utilises RanBP1 agarose beads to isolate selectively and pull-down the active form of Ran from purified samples or endogenous lysates. Subsequently, precipitated Ran-GTP was detected by western blot analysis using an anti-Ran antibody.

The Ran activation assay was performed by immunoprecipitation using anti–Ran binding protein 1 (RanBP1) antibody, which binds only to Ran-GTP in MDA-MB-231 cells. The resultant pull-down eluents were than analysed by immunoblotting for Ran. Four cell lysates were used, derived from (i) control cells, (ii) cells treated with blank NP, (iii) cells treated with free peptide and (iv) cells treated with peptide-loaded NP. Each cell lysate type was subjected to positive and negative controls.

2.12 Statistical analysis

Results are presented as mean ± standard deviation (SD) and analysed statistically using one-way analysis of variance (ANOVA) followed by Tukey's post hoc test. A value of $p < 0.05$ was considered statistically significant.

3. Results and Discussion

The physicochemical parameters of polymeric NP loaded with peptide, such as mean particle size, PDI, zeta potential and encapsulation efficiency are shown in Table 2. Optimisation was achieved by simultaneously minimising mean size and maximising peptide loading.

3.1 Effect of Polymer type

The effect of increasing PEG content in the PLGA backbone on physicochemical characterisation can be seen by comparing F1, F4 and F7. PLGA NP (F1) (330.0 ± 20.1 nm) were significantly larger in size ($p < 0.001$) than NP prepared from PEGylated polymers of F4 (250.2 ± 12.8 nm) and F7 (217.3 ± 11.1 nm) for 5 and 10% PEG-PLGA diblock copolymers, respectively (Fig. 1A). Covalently linked hydrophilic PEG blocks modify PLGA, producing smaller particles (Rojnik et al., 2012). All NP formulations were of low polydispersity index ranging from 0.26 to 0.39. Increasing the PEG fraction in the NP matrix resulted in a decrease in the mean NP diameter, which is a similar finding to that reported in other studies (Haggag et al., 2016).

The zeta potential of NP plays an important role in stability. F1 exhibited higher negative ζ-potential values (-18.9 ± 2.6 mV) compared to the PEGylated PLGA NP (F4 and F7) ($p < 0.001$) (Fig. 1B). Increasing the PEG fraction from 5% to 10% had no further effect. The PEG-PLGA NP had a lower negative zeta potential, relatively close to neutral, due to the presence of surface-located PEG chains that shield free carboxylic groups responsible for the overall negative particulate surface charge (Xiao et al., 2010).

Increasing PEG fraction in the polymer backbone resulted in a significant increase in peptide entrapment ($p < 0.01$). Encapsulation efficiency was increased from 37.0% ± 2.2% in PLGA to 54.9% ± 2.6% in 10% PEG-PLGA (Fig. 1C). In the diblock types, PEG chains orient themselves towards the aqueous phase in micelles, surrounding the encapsulated

peptide (Tobio et al., 1998). Hydrophilic microenvironments created by these PEG segments, produce regions that encapsulated peptide can occupy (Haggag et al., 2016), which facilitated high drug loading and encapsulation efficiency. Additionally, the higher encapsulation efficiency of 10% PEG-PLGA is due to its lower solubility in methylene chloride, which shortens solidification time and enhances encapsulation (Mehta et al., 1996).

The *in vitro* release profile showed that the burst release of peptide was faster and significantly higher ($p < 0.001$) from PEGylated PLGA NP when compared to PLGA NP. F4 and F7 released approximately 62.6% ± 2.5% and 70.4% ± 6% of peptide within the first 24 hours compared to 51.5% ± 1.5% released from F1 (Fig. 1D). Although release of peptide from PLGA NP was sustained over the experimental period, the PEGylated PLGA NP showed faster release of peptide immediately after incubation with release medium. Release then became slower, with approximately 90% of peptide released over 7 days in the PEGylated PLGA NP. Higher burst release can be attributed to peptide attached to the surface of the PEGylated PLGA NP. Moreover, hydrophilic PEG chains allowed faster release of the peptide through enhanced polymer degradation rate because water was taken up more readily when compared to PLGA NP (Locatelli and Comes Franchini, 2012). Overall, it can be concluded that PEGylation significantly affected physicochemical properties, such as size, shape, surface charge and surface hydrophobicity. These factors are known to influence NP uptake and biological activity in organ and tissue structures.

3.2 Effect of External aqueous phase volume

Three different external phase volumes (50, 75 and 100 ml) were used in this study to make NP comprising PLGA (F1, F2 and F3), 5% PEG-PLGA (F4, F5 and F6) and 10% PEG-PLGA (F7, F8 and F9). An increase in volume from 50 ml to 100 ml caused an insignificant increase in size ($p > 0.05$) of the PLGA NP (Fig. 2A) with a significant increase ($p < 0.001$)

in PDI from 0.26 ± 0.04 to 0.45 ± 0.02. However, a slight increase in PDI with a significant increase in size from 250 nm to 325 nm and from 217 nm to 274 nm was observed for 5% and 10% PEGylated PLGA NP, respectively. Conversely, the increase in external PVA solution to 100 ml resulted in a significant increase in size ($p < 0.01$) of 5% and 10% PEGylated PLGA NP from 250.3 ± 12.8 nm to 325.5 ± 27 nm and from 217.3 ± 11.1 nm to 274.8 ± 19.6 nm for 5% and 10% PEGylated PLGA NP, respectively. However, an insignificant decrease in PDI values ($p > 0.05$) was observed. A possible explanation is that increasing the external aqueous phase volume, resulted in reduced shear forces during the second emulsification step and, hence, reduced the mixing or dispersion efficiency needed to break the emulsion droplets effectively. This yielded larger emulsion droplets, which finally led to larger NP (Li, 1999). The reduced mixing can also explain the increase in PDI values.

Preparation of peptide-loaded NP with different volumes of the external aqueous phase had no significant effect on zeta potential ($p > 0.05$) (Fig. 2B). Encapsulation efficiency increased as the volume of the continuous phase increased (Fig. 2C). For example, when the ratio of dispersed phase to continuous phase (DP/CP) was decreased to 1/50, the encapsulation efficiency significantly increased ($p < 0.05$) by a factor of 36.9% (PLGA), 31.5% (5% PEG-PLGA) and 24.6% (10% PEG-PLGA) when compared to the higher DP/CP ratio of 1/25. It was likely that a large volume of continuous phase provides nearly a sink condition for diluting the organic solvent so that DCM was extracted promptly, resulting in fast solidification of the polymer that eventually led to higher entrapment (Mehta et al., 1996). *In vitro* release profiles showed that external phase volume influenced release, but PEGylation had a more pronounced effect. The profiles in Fig. 2D illustrate how volume variation affects release as polymer type is held constant (5% PEG-PLGA removed for clarity). For low external volume, the solidification process is expected to be slower. Water is then able to influx from either the aqueous phase (external and internal) into the polymer

structure, which creates water-filled channels or pores. Polymer solidification is expected to be faster for larger external volumes, as DCM is extracted more effectively. In such cases, a less porous structure is expected and release is slower (Jiang et al., 2002). It can be concluded that the external aqueous phase volume can be used to optimise NP physicochemical properties by controlling the NP size, encapsulation efficiency and *in vitro* release, which are essential parameters for effective nanoparticulate therapeutics.

3.3 Effect of peptide loading

Three different peptide loadings were used in this study (6%, 4% and 2%), as shown in Fig. 3. Decreasing peptide loading resulted in a non-significant decrease in the size of PLGA NP ($p > 0.05$) (Fig. 3A). However, decreasing the peptide loading from 6% to 2% in PEG-PLGA formulations resulted in a significant decrease in NP size ($p < 0.001$). NP size decreased from 325.5 ± 27 nm to 178.5 ± 25.7 nm and from 274.8 ± 19.6 nm to 161.8 ± 15.7 nm for 5% and 10% PEGylated NP, respectively. It is feasible that increasing the peptide loading increased the amount bound to the NP surface due to the presence of PEG moieties. But given that the amount of peptide in comparison to the total polymer is low, increases in loading from 2% to 6% are unlikely to push much more peptide to the surface. Furthermore, the zeta potential data in Fig. 3B show no evidence of charge shielding from increasing surface peptide. It is feasible that these results highlight a different peptide packing mechanism in the NP matrix when PEGylated PLGA types are compared to PLGA-only matrices.

PDI values reduced following a decrease in peptide loading, with no significant effect on the surface charge (Fig. 3B). Peptide loading had a significant impact of on the encapsulation efficiency in all types of NP. The decrease in peptide loading resulted in a significant increase in encapsulation efficiency ($p < 0.05$) (Fig. 3C). Of particular interest are

the optimised encapsulation efficiencies observed for 10% PEG-PLGA NP, which increased from 68.4% ± 2.1% to 80.5% ± 6.1%.

The release profiles and the initial bursts were closely related to the degree of peptide loading (Fig.3D). The release profile of F3, F6 and F9 with a loading of 2% was significantly lower than those of 6% loading ($p < 0.01$). Initial bursts of 41.4% ± 2.2%, 52.5% ± 3.2% and 59.4% ± 2.0% were observed from F3, F6 and F9, respectively, compared to 31.5% ± 1.0%, 40.3% ± 1.5% and 45.5% ± 1.5% from F11, F13 and F15, respectively. Using increased amounts of peptide in the primary emulsion droplets enhanced the concentration gradient acting towards the external water phase, which led to increased outward diffusion (Lamprecht et al., 2000). Moreover, there is likely to be more peptide distributed near the NP surface, especially for PEGylated PLGA NP. The diffusion of surface-associated peptide facilitated the formation of water-filled channels that allow subsequent elution of the remaining peptide located inside the NP. This leads to a greater initial release (Yang et al., 2001).

3.4 Effect of peptide charge

In this study, peptide was dissolved in two aqueous solvent types (PBS and 0.1 M HCl pH 1.0) to investigate the effect of electrostatic interaction on the physicochemical characterisation of different NP formulations of PLGA (F11 and F16), 5% PEG-PLGA (F13 and F17) and 10% PEG-PLGA (F15 and F18). Anti-Ran-GTPase peptide is a neutral peptide with an isoelectric point (p*I*) around 6.0 (Gasteiger E., 2005). Peptide dissolved in PBS is unlikely to interact with the PLGA. However, in 0.1 M HCl, the peptide is cationic and an objective in this part of the study was to investigate interaction with uncapped carboxylic acid terminal end groups.

The predicted peptide-polymer interaction had no significant impact on NP size and PDI (Fig. 4A), although there was evidence that it influenced the zeta potential ($p > 0.05$)

(Fig. 4B). Conversely, interaction between peptide and polymer contributed to increasing encapsulation efficiency, which was observed in all polymer types. However, a sharp increase in peptide encapsulation efficiency was observed for PLGA ($p < 0.001$), which exceeded that for the other PEGylated polymers (Fig. 4C). The abundance of free carboxyl groups, which are more prevalent in PLGA, would explain this observation. Interestingly, the free carboxyl group is not expected to be charged in DCM or 0.1 M HCl, as used in this work, but there is evidence of an interaction that enhances encapsulation, as seen in Fig. 4C. This interaction would retard peptide diffusivity to the external aqueous phase during the preparation process and impede unwanted loss (Fude et al., 2005). Encapsulation of cationic peptides within uncapped polymers that carry free carboxylic end groups is preferable to the end-capped variants.

In vitro release profiles of PLGA NP showed a reduced initial burst release phase, when compared to profiles in Fig 1D, followed by a slower release profile during the remainder of the incubation period (Fig. 4D). Strong interactions between polymer and peptide are predicted to influence release from the final delivery system (Kim and Park, 1999). Indeed, further work done in this study with alteration in the ionic strength of the release medium (data not shown) was able to reverse the reduction of release rates. Increases in ionic strength of the medium reduces the extent of ionic interaction by shielding charged groups (Park et al., 1998). These results support a peptide release mechanism from PLGA NP that is not only controlled by degradation or erosion of the polymer, but also due to the possible electrostatic interactions. This reduction in initial burst is viewed as advantageous, as it minimises the risk of premature *in vivo* release. A nanoparticulate system intended for cytosolic delivery must reach that location before significant drug release has occurred.

Although interactions of the type described above may adapt the release rate in a favourable way, there is risk that stability of the peptide is adversely affected. Structural

stability was assured by mass spectroscopic data, which confirmed that the peptide mass was unaltered following *in vitro* release after seven days from F18 (Fig. 5A). Furthermore, HPLC data did not show changes in retention time during the same time period.

3.5 Scanning electron microscopy

To access the surface morphology, aggregation or adhesion of peptide-loaded NP (F18), SEM was used to visualise the particulate surface. SEM images revealed a smooth spherical shape of homogenous size, with no evidence of particle adhesion or aggregation (Fig 5B). The average size obtained from SEM was comparable to what obtained by laser diffraction. After 7 days of *in vitro* release, exhausted NP samples appeared to have a more porous and labyrinthine structure. This structure would result from drug diffusion after the erosion of the polymer by the aqueous release media (Haggag et al., 2016) (Fig. 5C).

3.6 Cellular uptake of nanoparticles

An objective of this study was to investigate the efficiency of cellular uptake of PLGA and PEGylated PLGA NP by MDA-MB231 breast cancer cells. Quantitative flow cytometry analysis, after 24 hours of treatment, showed that the percentage of cells with positive staining following treatment with 10% PEGylated NP was significantly higher ($p < 0.001$) than all other NP formulations made from PLGA and 5% PEG-PLGA. F18 induced the best cellular uptake with 54.8% ± 12.7% positive cells, compared to 11.4% ± 3.7% and 18.1% ± 7.3% for F16 and F17, respectively. These results showed that F18, with the lowest particle size (162 nm), highest PEG content and lowest zeta potential (−4.5 mV) gave rise to the greatest uptake by MDA-MB-231 cells (Fig. 6). Quantitative uptake data for F18 clearly demonstrated its superiority over other formulations, such as F16 and F17, and so this formulation was investigated further.

Fluorescence microscopy studies provided limited evidence of F18 uptake in MDA-MB-231 cells (Fig. 7). It is possible that fixation, as used in this work, may have contributed to this low level of visual data (Richard et al., 2003). However, peptide-loaded NP were seen to be primarily localised in the cytoplasmic compartment, while some fluorescence intensity was observed in the perinuclear region (Fig. 7G-7I). Coumarin 6 uptake from solution showed minimal internalisation (Fig. 7D-7F). The efficiency of cellular internalisation of nanoparticles is known to be dependent on their diameter (Kamaly et al., 2012) and for the purposes of tumour accumulation, the upper limit for extravasation into solid tumours is suggested to be approximately 400 nm. It is generally observed that NP below 200 nm accumulate effectively within tumour tissue, with the 70–200 nm range considered optimal for tumour passive targeting (Torchilin, 2007). Therefore, the diameter observed for F18 fits well within this optimal range.

The benefits of PEG on prolonging circulation time of colloidal carriers are well known (Cruje and Chithrani, 2015), but in this study, however, it is the role of PEG as a component part of the particulate matrix on cellular uptake that is of particular importance. Its effect is clearly demonstrated in Fig. 6 and, based on quantitative and qualitative results, it was concluded that 10% PEGylated PLGA NP showed optimised cellular uptake. This finding is generally supported in the literature (Pamujula et al., 2012), where increasing levels of PEG gives rise to NP with favourable characteristics, such as enhanced internalisation. There are reports that contradict this finding and propose that PEG will repel nanocarriers from the cell surface (Pelaz et al., 2015). On balance, the results of this current study support the enhanced internalisation effect. Moreover, localisation of peptide-loaded NP in the cytoplasm, where Ran GDP is localised, is desirable as it is the most effective site for delivery of the blockade peptide. Successful translocation of NP from endosome to cytoplasm is an essential demand of any polymer-mediated drug delivery system as bio-therapeutics

must be localised in the cytosol to exert functional activity. The need of NP to escape the endosome prior to fusion with lysosomes is the most important step in reaching the desired subcellular compartments (Whitehead et al., 2009). Reversal of the surface charge of related PLGA NP via transfer of protons/hydronium ions by the aid of acidic pH of endo-lysosomes is the proposed mechanism for endo-lysosomal escape (Makino et al., 1986). Based on cellular uptake results in the test cell line, F18 was selected for further studies.

3.7 In vitro cytotoxicity and cell cycle analysis

The cytotoxic action of peptide-loaded NP on the MDA-MB-231 cell line was evaluated using MTT assay after 24, 48, 72 and 96 hours of treatment at 2, 4 and 8 µM of free peptide and peptide-loaded NP (F18). Dose effect curves were used to detect the drug concentration that caused 50% growth inhibition (IC_{50}). The results showed that the blank NP and free peptide had no cytotoxicity on breast cancer cells within the concentration range used (Fig. 8). Peptide-loaded NP reduced cell viability and a sustained cytotoxic action was achieved for up to four days after treatment. The mean IC_{50} value for peptide-loaded 10% PEG-PLGA NP in MDA-MB-231 cells was 3.6 µM, which was achieved within 24 hours. Based on these findings, the free peptide does not achieve any cytotoxic effect, which confirms our previous findings. This is due to poor delivery to the site of action or possible degradation. However, NP were able to deliver peptide to its subcellular site, protected it from degradation and induced cytotoxicity, mostly likely by deactivation of Ran-GTP formation.

The results of cell cycle analysis showed that cells treated with peptide-loaded NP were arrested at the mitotic division stage of the G0/G1 and G2/M phase. Peptide-loaded NP showed a stronger effect after 48 hours. Peptide-loaded NP at concentrations of 4 and 8 µM caused significantly higher G0/G1 phase arrest of 31.2% and 55.4% after 48 hours, compared to results after 24 hours of 14.2% and 37.7%, respectively, using similar concentrations (Fig.

9). Concomitantly, the growth rate of the cells was also reduced after peptide-loaded NP treatment, whereas cells treated with free peptide were not affected. This confirmed the peptide blockade effect on Ran by inhibition of Ran-GTP formation and its role in cell mitosis.

3.8 Ran activation assay

Ran regulates molecular events by cycling between an inactive GDP-bound form and an active GTP-bound form. In its active (GTP-bound) state, Ran binds specifically to RanBP1 to control downstream signaling cascades. These results led us to investigate if the peptide delivered from the loaded NP is specifically inhibiting Ran activation by preventing its conversion from Ran-GDP to Ran-GTP. The important band to note in Fig. 10 is lane 5 in panel B, which is the lysate of cells treated with peptide-loaded NP. There is clear evidence of inhibition of Ran-GTP formation which is the active form (2.5 fold decrease) when compared to free peptide- treated cells (lane 2 in panel B). These results confirm that our anti-Ran-GTPase peptide is delivered effectively to the cytoplasm and retains it functional interaction with Ran-GDP, causing subsequent inhibition of Ran activation.

Conclusions

There is accumulating evidence that Ran is overexpressed in breast tumours and high levels lead to increased cancer cell invasion and metastasis *in vivo*. Developing novel Ran targeted therapies, such as an anti-Ran-GTPase peptide, is an attractive therapeutic approach. Due to the poor bioavailability and ineffective delivery of naked Ran interfering peptides, we sought to improve delivery by NP encapsulation. Optimisation of the physicochemical properties of peptide-loaded NP can directly affect its physical stability, drug release, cellular uptake and

the therapeutic activity. Low peptide loading, low DP/CP ratio and peptide polymer ionic interaction resulted in the formulation of spherical, peptide-loaded NP with high encapsulation efficiency, low size range, low PDI and a low negative zeta potential providing more rapid intracellular entry. Mass spectroscopy revealed that the peptide was incorporated and released from the NP without altering its molecular weight. The therapeutic efficacy of the peptide-loaded NP largely depended on the availability at the intracellular site of action. Our results from intracellular uptake studies demonstrated a rapid and pronounced cellular uptake of PEGylated NP, due mostly to the presence of PEG, resulting in increased preferential cytotoxicity in a model cancer cell line. Peptide-loaded NP exhibited an IC_{50} at a low dose of 3.6 µM in breast cancer cells. Free peptide had a negligible cytotoxic effect on cells, confirming the peptide displayed preferential sensitivity once intracellular delivery was facilitated. Nanoparticles encapsulating the anti-Ran peptide inhibited Ran-GTP formation which is essential for tumorigenesis and metastasis. Peptide-loaded PEG-PLGA NP proved to be an effective nanoparticulate delivery system and it may represent a novel anti-metastatic drug candidate for therapeutic benefit in invasive breast cancers.

References

Abe, H., Kamai, T., Shirataki, H., Oyama, T., Arai, K., Yoshida, K., 2008. High expression of Ran GTPase is associated with local invasion and metastasis of human clear cell renal cell carcinoma. International journal of cancer. Journal international du cancer 122, 2391-2397.

Aina, O.H., Sroka, T.C., Chen, M.L., Lam, K.S., 2002. Therapeutic cancer targeting peptides. Biopolymers 66, 184-199.

Alcock, R., Blair, J.A., O'Mahony, D.J., Raoof, A., Quirk, A.V., 2002. Modifying the release of leuprolide from spray dried OED microparticles. Journal of Controlled Release 82, 429-440.

Angelov, B., Angelova, A., Papahadjopoulos-Sternberg, B., Hoffmann, S.V., Nicolas, V., Lesieur, S., 2012. Protein-Containing PEGylated Cubosomic Particles: Freeze-Fracture Electron Microscopy and Synchrotron Radiation Circular Dichroism Study. The Journal of Physical Chemistry B 116, 7676-7686.

Angelova, A., Angelov, B., Drechsler, M., Garamus, V.M., Lesieur, S., 2013a. Protein entrapment in PEGylated lipid nanoparticles. International journal of pharmaceutics 454, 625-632.

Angelova, A., Angelov, B., Drechsler, M., Lesieur, S., 2013b. Neurotrophin delivery using nanotechnology. Drug discovery today 18, 1263-1271.

Angelova, A., Angelov, B., Mutafchieva, R., Lesieur, S., 2015. Biocompatible Mesoporous and Soft Nanoarchitectures. Journal of Inorganic and Organometallic Polymers and Materials 25, 214-232.

Angelova, A., Angelov, B., Mutafchieva, R., Lesieur, S., Couvreur, P., 2011. Self-assembled multicompartment liquid crystalline lipid carriers for protein, peptide, and nucleic acid drug delivery. Accounts of chemical research 44, 147-156.

Anthony, L., Freda, P.U., 2009. From somatostatin to octreotide LAR: evolution of a somatostatin analogue. Current medical research and opinion 25, 2989-2999.

Bischoff, F.R., Ponstingl, H., 1991a. Catalysis of guanine nucleotide exchange on Ran by the mitotic regulator RCC1. Nature 354, 80-82.

Bischoff, F.R., Ponstingl, H., 1991b. Mitotic regulator protein RCC1 is complexed with a nuclear ras-related polypeptide. Proceedings of the National Academy of Sciences of the United States of America 88, 10830-10834.

Borghouts, C., Kunz, C., Groner, B., 2005. Current strategies for the development of peptide-based anti-cancer therapeutics. Journal of Peptide Science 11, 713-726.

Brigger, I., Dubernet, C., Couvreur, P., 2002. Nanoparticles in cancer therapy and diagnosis. Advanced drug delivery reviews 54, 631-651.

Crawford, E.D., Phillips, J.M., 2011. Six-month gonadotropin releasing hormone (GnRH) agonist depots provide efficacy, safety, convenience, and comfort. Cancer management and research 3, 201-209.

Cruje, C., Chithrani, B.D., 2015. Integration of Peptides for Enhanced Uptake of PEGylayed Gold Nanoparticles. Journal of nanoscience and nanotechnology 15, 2125-2131.

Enbäck, J., Laakkonen, P., 2007. Tumour-homing peptides: tools for targeting, imaging and destruction.

Fude, C., Dongmei, C., Anjin, T., Mingshi, Y., Kai, S., Min, Z., Ying, G., 2005. Preparation and characterization of melittin-loaded poly (dl-lactic acid) or poly (dl-lactic-co-glycolic acid) microspheres made by the double emulsion method. Journal of Controlled Release 107, 310-319.

Gasteiger E., H.C., Gattiker A., Duvaud S., Wilkins M.R., Appel R.D., Bairoch A, 2005. Protein Identification and Analysis Tools on the ExPASy Server. Humana Press.

Haggag, Y., Abdel-Wahab, Y., Ojo, O., Osman, M., El-Gizawy, S., El-Tanani, M., Faheem, A., McCarron, P., 2016. Preparation and in vivo evaluation of insulin-loaded biodegradable nanoparticles prepared from diblock copolymers of PLGA and PEG. International journal of pharmaceutics 499, 236-246.

Haggag, Y.A., Faheem, A.M., 2015. Evaluation of nano spray drying as a method for drying and formulation of therapeutic peptides and proteins. Frontiers in Pharmacology 6, 140.

Jain, R.A., 2000. The manufacturing techniques of various drug loaded biodegradable poly(lactide-co-glycolide) (PLGA) devices. Biomaterials 21, 2475-2490.

Jiang, G., Thanoo, B.C., DeLuca, P.P., 2002. Effect of osmotic pressure in the solvent extraction phase on BSA release profile from PLGA microspheres. Pharmaceutical development and technology 7, 391-399.

Kamaly, N., Xiao, Z., Valencia, P.M., Radovic-Moreno, A.F., Farokhzad, O.C., 2012. Targeted polymeric therapeutic nanoparticles: design, development and clinical translation. Chemical Society reviews 41, 2971-3010.

Kim, H.K., Park, T.G., 1999. Microencapsulation of human growth hormone within biodegradable polyester microspheres: protein aggregation stability and incomplete release mechanism. Biotechnology and bioengineering 65, 659-667.

Kurisetty, V.V., Johnston, P.G., Johnston, N., Erwin, P., Crowe, P., Fernig, D.G., Campbell, F.C., Anderson, I.P., Rudland, P.S., El-Tanani, M.K., 2008. RAN GTPase is an effector of the invasive/metastatic phenotype induced by osteopontin. Oncogene 27, 7139-7149.

Labhasetwar, V., 1997. Nanoparticles for drug delivery. Pharm. News 4, 28–31.

Lamprecht, A., Ubrich, N., Hombreiro Perez, M., Lehr, C., Hoffman, M., Maincent, P., 2000. Influences of process parameters on nanoparticle preparation performed by a double emulsion pressure homogenization technique. International journal of pharmaceutics 196, 177-182.

Li, X., 1999. Investigation on process parameters involved in preparation of poly-?-lactide-poly(ethylene glycol) microspheres containing Leptospira Interrogans antigens. International journal of pharmaceutics 178, 245-255.

Locatelli, E., Comes Franchini, M., 2012. Biodegradable PLGA-b-PEG polymeric nanoparticles: synthesis, properties, and nanomedical applications as drug delivery system. J Nanopart Res 14, 1-17.

Looi, C.Y., Imanishi, M., Takaki, S., Sato, M., Chiba, N., Sasahara, Y., Futaki, S., Tsuchiya, S., Kumaki, S., 2011. Octa-Arginine Mediated Delivery of Wild-Type Lnk Protein Inhibits TPO-Induced M-MOK Megakaryoblastic Leukemic Cell Growth by Promoting Apoptosis. PLoS ONE 6, e23640.

Ly, T.K., Wang, J., Pereira, R., Rojas, K.S., Peng, X., Feng, Q., Cerione, R.A., Wilson, K.F., 2010. Activation of the Ran GTPase is subject to growth factor regulation and can give rise to cellular transformation. The Journal of biological chemistry 285, 5815-5826.

Makino, K., Ohshima, H., Kondo, T., 1986. Transfer of protons from bulk solution to the surface of poly(L-lactide) microcapsules. Journal of microencapsulation 3, 195-202.

Matchett, K.B., McFarlane, S., Hamilton, S.E., Eltuhamy, Y.S., Davidson, M.A., Murray, J.T., Faheem, A.M., El-Tanani, M., 2014. Ran GTPase in nuclear envelope formation and cancer metastasis. Advances in experimental medicine and biology 773, 323-351.

Mehta, R.C., Thanoo, B.C., Deluca, P.P., 1996. Peptide containing microspheres from low molecular weight and hydrophilic poly(d,l-lactide-co-glycolide). Journal of Controlled Release 41, 249-257.

Ohtsubo, M., Okazaki, H., Nishimoto, T., 1989. The RCC1 protein, a regulator for the onset of chromosome condensation locates in the nucleus and binds to DNA. The Journal of cell biology 109, 1389-1397.

Palmer, T.D., Ashby, W.J., Lewis, J.D., Zijlstra, A., 2011. Targeting tumor cell motility to prevent metastasis. Advanced drug delivery reviews 63, 568-581.

Pamujula, S., Hazari, S., Bolden, G., Graves, R.A., Chinta, D.D., Dash, S., Kishore, V., Mandal, T.K., 2012. Cellular delivery of PEGylated PLGA nanoparticles. The Journal of pharmacy and pharmacology 64, 61-67.

Park, T.G., Yong Lee, H., Sung Nam, Y., 1998. A new preparation method for protein loaded poly(d,l-lactic-co-glycolic acid) microspheres and protein release mechanism study. Journal of Controlled Release 55, 181-191.

Pelaz, B., del Pino, P., Maffre, P., Hartmann, R., Gallego, M., Rivera-Fernandez, S., de la Fuente, J.M., Nienhaus, G.U., Parak, W.J., 2015. Surface Functionalization of Nanoparticles with Polyethylene Glycol: Effects on Protein Adsorption and Cellular Uptake. ACS Nano 9, 6996-7008.

Renault, L., Kuhlmann, J., Henkel, A., Wittinghofer, A., 2001. Structural Basis for Guanine Nucleotide Exchange on Ran by the Regulator of Chromosome Condensation (RCC1). Cell 105, 245-255.

Richard, J.P., Melikov, K., Vives, E., Ramos, C., Verbeure, B., Gait, M.J., Chernomordik, L.V., Lebleu, B., 2003. Cell-penetrating peptides. A reevaluation of the mechanism of cellular uptake. J. Biol. Chem. 278, 585-590.

Rojnik, M., Kocbek, P., Moret, F., Compagnin, C., Celotti, L., Bovis, M.J., Woodhams, J.H., Macrobert, A.J., Scheglmann, D., Helfrich, W., Verkaik, M.J., Papini, E., Reddi, E., Kos, J., 2012. In vitro and in vivo characterization of temoporfin-loaded PEGylated PLGA nanoparticles for use in photodynamic therapy. Nanomedicine (London, England) 7, 663-677.

Rush, M.G., Drivas, G., D'Eustachio, P., 1996. The small nuclear GTPase Ran: How much does it run? BioEssays 18, 103-112.

Sazer, S., 1996. The search for the primary function of the Ran GTPase continues. Trends in cell biology 6, 81-85.

Scheffzek, K., Klebe, C., Fritz-Wolf, K., Kabsch, W., Wittinghofer, A., 1995. Crystal structure of the nuclear Ras-related protein Ran in its GDP-bound form. Nature 374, 378-381.

Sethi, R., Sanfilippo, N., 2009. Six-month depot formulation of leuprorelin acetate in the treatment of prostate cancer. Clinical Interventions in Aging 4, 259-267.

Sharma, A., Jain, N., Sareen, R., 2013. Nanocarriers for diagnosis and targeting of breast cancer. BioMed research international 2013, 960821.

Thayer, A.M., 2011. IMPROVING PEPTIDES. Chemical & Engineering News Archive 89, 13-20.

Tobio, M., Gref, R., Sanchez, A., Langer, R., Alonso, M.J., 1998. Stealth PLA-PEG nanoparticles as protein carriers for nasal administration. Pharm Res 15, 270-275.

Torchilin, V.P., 2007. Targeted pharmaceutical nanocarriers for cancer therapy and imaging. The AAPS journal 9, E128-147.

Vetter, I.R., Nowak, C., Nishimoto, T., Kuhlmann, J., Wittinghofer, A., 1999. Structure of a Ran-binding domain complexed with Ran bound to a GTP analogue: implications for nuclear transport. Nature 398, 39-46.

Vlieghe, P., Lisowski, V., Martinez, J., Khrestchatisky, M., 2010. Synthetic therapeutic peptides: science and market. Drug discovery today 15, 40-56.

West, C.P., Lumsden, M.A., Lawson, S., Williamson, J., Baird, D.T., 1987. Shrinkage of uterine fibroids during therapy with goserelin (Zoladex): a luteinizing hormone-releasing hormone agonist administered as a monthly subcutaneous depot. Fertility and sterility 48, 45-51.

Whitehead, K.A., Langer, R., Anderson, D.G., 2009. Knocking down barriers: advances in siRNA delivery. Nature reviews. Drug discovery 8, 129-138.

Xia, F., Lee, C.W., Altieri, D.C., 2008. Tumor cell dependence on Ran-GTP-directed mitosis. Cancer research 68, 1826-1833.

Xiao, R.Z., Zeng, Z.W., Zhou, G.L., Wang, J.J., Li, F.Z., Wang, A.M., 2010. Recent advances in PEG-PLA block copolymer nanoparticles. International journal of nanomedicine 5, 1057-1065.

Yang, Y.Y., Chung, T.S., Ng, N.P., 2001. Morphology, drug distribution, and in vitro release profiles of biodegradable polymeric microspheres containing protein fabricated by double-emulsion solvent extraction/evaporation method. Biomaterials 22, 231-241.

Yuen, H.F., Chan, K.K., Grills, C., Murray, J.T., Platt-Higgins, A., Eldin, O.S., O'Byrne, K., Janne, P., Fennell, D.A., Johnston, P.G., Rudland, P.S., El-Tanani, M., 2012. Ran is a potential therapeutic target for cancer cells with molecular changes associated with activation of the PI3K/Akt/mTORC1 and Ras/MEK/ERK pathways. Clinical cancer research : an official journal of the American Association for Cancer Research 18, 380-391.

Yuen, H.F., Gunasekharan, V.K., Chan, K.K., Zhang, S.D., Platt-Higgins, A., Gately, K., O'Byrne, K., Fennell, D.A., Johnston, P.G., Rudland, P.S., El-Tanani, M., 2013. RanGTPase: a candidate for Myc-mediated cancer progression. Journal of the National Cancer Institute 105, 475-488.

Figure legends

Figure 1. Effects of polymer type on NP size (A), zeta potential (B), encapsulation efficiency (C) and *in vitro* release (D). Values are mean ± SD with n = 3. For 1A-1C, *p < 0.05, **p < 0.01, ***p < 0.001 compared with PLGA. $^{\Delta}$p < 0.05 compared with 5% PEG-PLGA.

Figure 2. Effects of external aqueous phase volume on (A) NP size, (B) zeta potential, (C) encapsulation efficiency and (D) *in vitro* peptide release. Values are mean ± SD with n = 3. For 2A-2C, *p < 0.05, **p < 0.01, ***p < 0.001 compared with 50 ml for each polymer type. $^{\Delta}$ p < 0.05, $^{\Delta\Delta}$ p < 0.01, $^{\Delta\Delta\Delta}$ p < 0.001 compared with 75 ml for each polymer type.

Figure 3. Effects of peptide loading on (A) NP size, (B) zeta potential, (C) encapsulation efficiency and (D) in vitro peptide release. Values are mean ± SD with n = 3. For 3A-3C, *p < 0.05, **p < 0.01, ***p < 0.001 compared with 6% peptide loading for each polymer type. Δ p < 0.05, ΔΔ p < 0.01, ΔΔΔ p < 0.001 compared with 4% peptide loading for each polymer type.

Figure 4. Effects of peptide polymer interaction on (A) NP size, (B) zeta potential, (C) encapsulation efficiency and (D) *in vitro* peptide release. Values are mean ± SD with n = 3. For 4A-4C, *p < 0.05, **p < 0.01, ***p < 0.001 compared with PBS for each polymer type.

Figure 5. SEM images of peptide-loaded NP (F18) (A) after formulation and (B) after 7 days of *in vitro* release, together with (C) the electron spray mass spectrum of peptide release after 7 days.

Figure 6. Quantitative cellular uptake of different types of peptide-loaded NP after 24 hours, as determined by flow cytometry. Values are mean + SD with n = 3. *** p < 0.001 compared with all other treatments.

Figure 7. Fluorescence microscope images of control cells (A-C), cells treated with coumarin 6 (D-F) and coumarin 6-loaded, peptide-loaded NP (F18) (G-I) after 24 hours of treatment.

Figure 8. MDA-MB-231 Cell viability results of different doses of free peptide and peptide-loaded NP after 24, 48, 72 and 96 hours.

Figure 9. MDA-MB-231 Cell cycle analysis results of different doses of free peptide and peptide-loaded NP after 24 and 48 hours.

Figure 10. (A) Immunoblotting results of control cells and cells treated with blank NP. *Lane 1* immunoblot positive control. *Lane 2*, cell lysate from control cells. *Lane 3*, control cell lysate spiked with GDP (negative control). *Lane 4*, control cell lysate spiked with GTPγS (positive control). *Lane 5*, cell lysate following treatment with blank NP. *Lane 6*, cell lysate following treatment with blank NP and spiked with GDP. *Lane 7*, cell lysate following treatment with blank NP and spiked with GTPγS.

(B) Immunoblotting results of cells treated with free peptide and cells treated with peptide-loaded NP. *Lane 1*, immunoblot positive control. *Lane 2*, cell lysate following treatment with free peptide. *Lane 3*, cell lysate following treatment with free peptide and spiked with GDP. *Lane 4*, cell lysate following treatment with free peptide and spiked with GTPγS. *Lane 5*, cell lysate following treatment with peptide-loaded NP. *Lane 6*, cell lysate following treatment with peptide-loaded NP and spiked with GDP. *Lane 7*, cell lysate following treatment with peptide-loaded NP and spiked with GTPγS.

Table 1. Process variables for peptide-loaded NP and corresponding identifiers

Formulation identifier	PEG content (polymer type)	Peptide Loading (%)	Internal aqueous phase Solvent*	External aqueous phase volume (ml)
F1	0% (PLGA)	6	PBS	50
F2	0% (PLGA)	6	PBS	75
F3	0% (PLGA)	6	PBS	100
F4	5% (PEG-PLGA)	6	PBS	50
F5	5% (PEG-PLGA)	6	PBS	75
F6	5% (PEG-PLGA)	6	PBS	100
F7	10% (PEG-PLGA)	6	PBS	50
F8	10% (PEG-PLGA)	6	PBS	75
F9	10% (PEG-PLGA)	6	PBS	100
F10	0% (PLGA)	4	PBS	100
F11	0% (PLGA)	2	PBS	100
F12	5% (PEG-PLGA)	4	PBS	100
F13	5% ((PEG-PLGA)	2	PBS	100
F14	10% (PEG-PLGA)	4	PBS	100
F15	10% (PEG-PLGA)	2	PBS	100
F16	0% (PLGA)	2	0.1 M HCl	100
F17	5% (PEG-PLGA)	2	0.1 M HCl	100
F18	10% (PEG-PLGA)	2	0.1 M HCl	100

*PBS – phosphate buffered saline (pH 7.4)

Table 2. Effects of different process variables on peptide-loaded NP size, PDI, zeta potential and encapsulation efficiency.

Formulation ID	Size (nm)*	PDI*	Zeta Potential (-mV)*	Encapsulation Efficiency (%)*
F1	330.0 ± 20.1	0.26 ± 0.04	-18.90 ± 2.60	36.99 ± 2.19
F2	355.0 ± 21.6	0.34 ± 0.03	-19.15 ± 2.07	43.99 ± 4.47
F3	363.5 ± 4.6	0.45 ± 0.03	-20.53 ± 1.91	50.66 ± 4.38
F4	250.3 ± 12.8	0.39 ± 0.03	-4.91 ± 1.29	45.56 ± 0.78
F5	265.3 ± 26.2	0.41 ± 0.02	-5.41 ± 0.92	49.23 ± 2.88
F6	325.3 ± 26.9	0.41 ± 0.03	-5.43 ± 1.72	59.89 ± 6.89
F7	217.3 ± 11.1	0.31 ± 0.02	-5.05 ± 1.17	54.88 ± 2.64
F8	225.0 ± 16.7	0.33 ± 0.01	-5.55 ± 0.98	58.88 ± 8.62
F9	274.8 ± 19.6	0.34 ± 0.02	-6.28 ± 1.92	68.39 ± 2.09
F10	327.5 ± 21.5	0.44 ± 0.02	-18.90 ± 2.55	59.66 ± 2.36
F11	312.5 ± 39.3	0.42 ± 0.03	-19.53 ± 2.71	67.66 ± 6.86
F12	247.8 ± 16.3	0.38 ± 0.03	-4.91 ± 1.29	68.98 ± 3.28
F13	178.5 ± 25.7	0.39 ± 0.03	-5.61 ± 2.19	77.50 ± 3.11
F14	210.0 ± 31.3	0.32 ± 0.02	-5.05 ± 1.17	73.87 ± 4.16
F15	161.8 ± 15.7	0.30 ± 0.03	-6.11 ± 2.39	80.52 ± 6.08
F16	276.5 ± 12.3	0.40 ± 0.02	-15.65 ± 2.35	93.66 ± 2.59
F17	196.0 ± 19.5	0.36 ± 0.05	-3.31 ± 1.62	86.50 ± 2.51
F18	181.8 ± 8.5	0.31 ± 0.03	-4.51 ± 2.12	90.19 ± 1.76

*All values are mean ± SD with n=3

Figure(s)

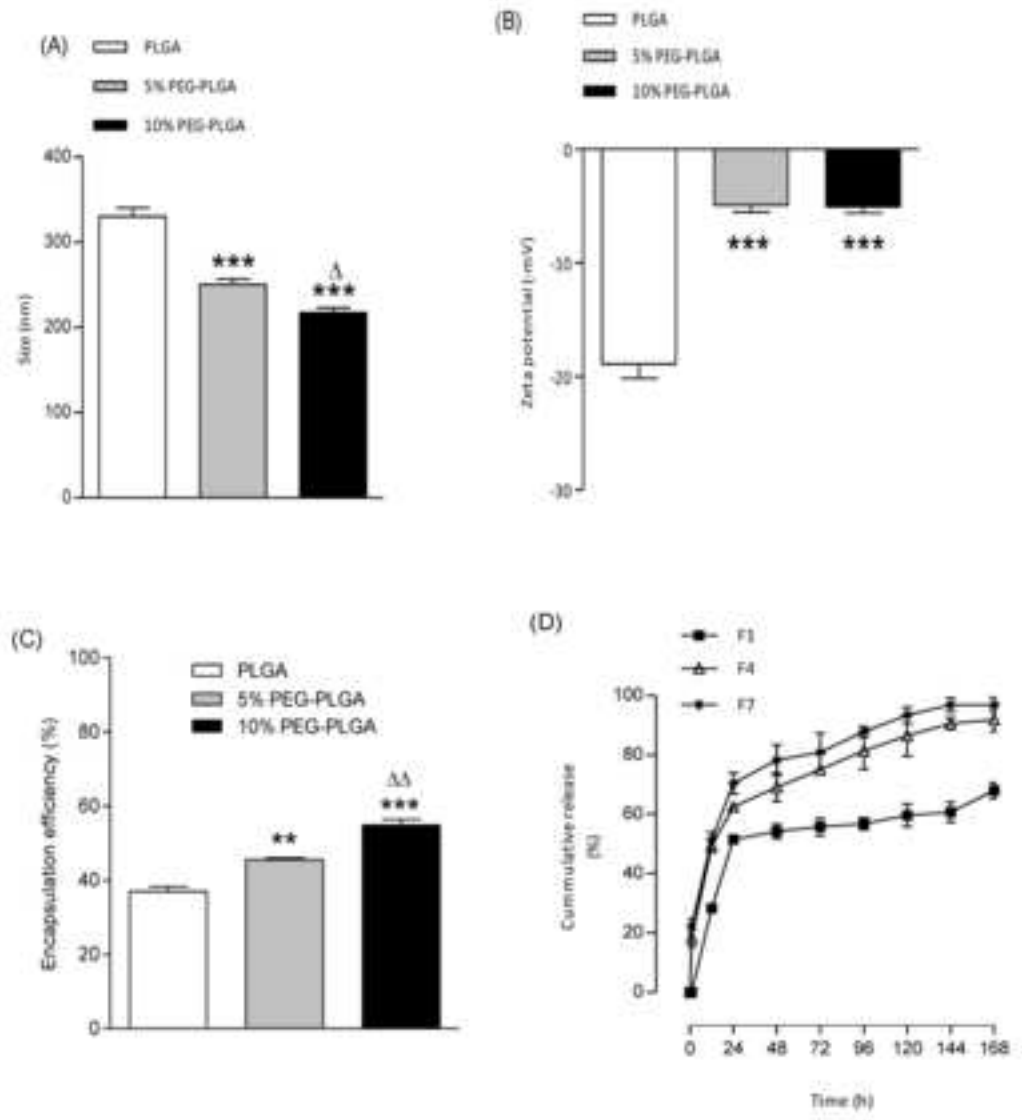

Figure 1.

Figure 2

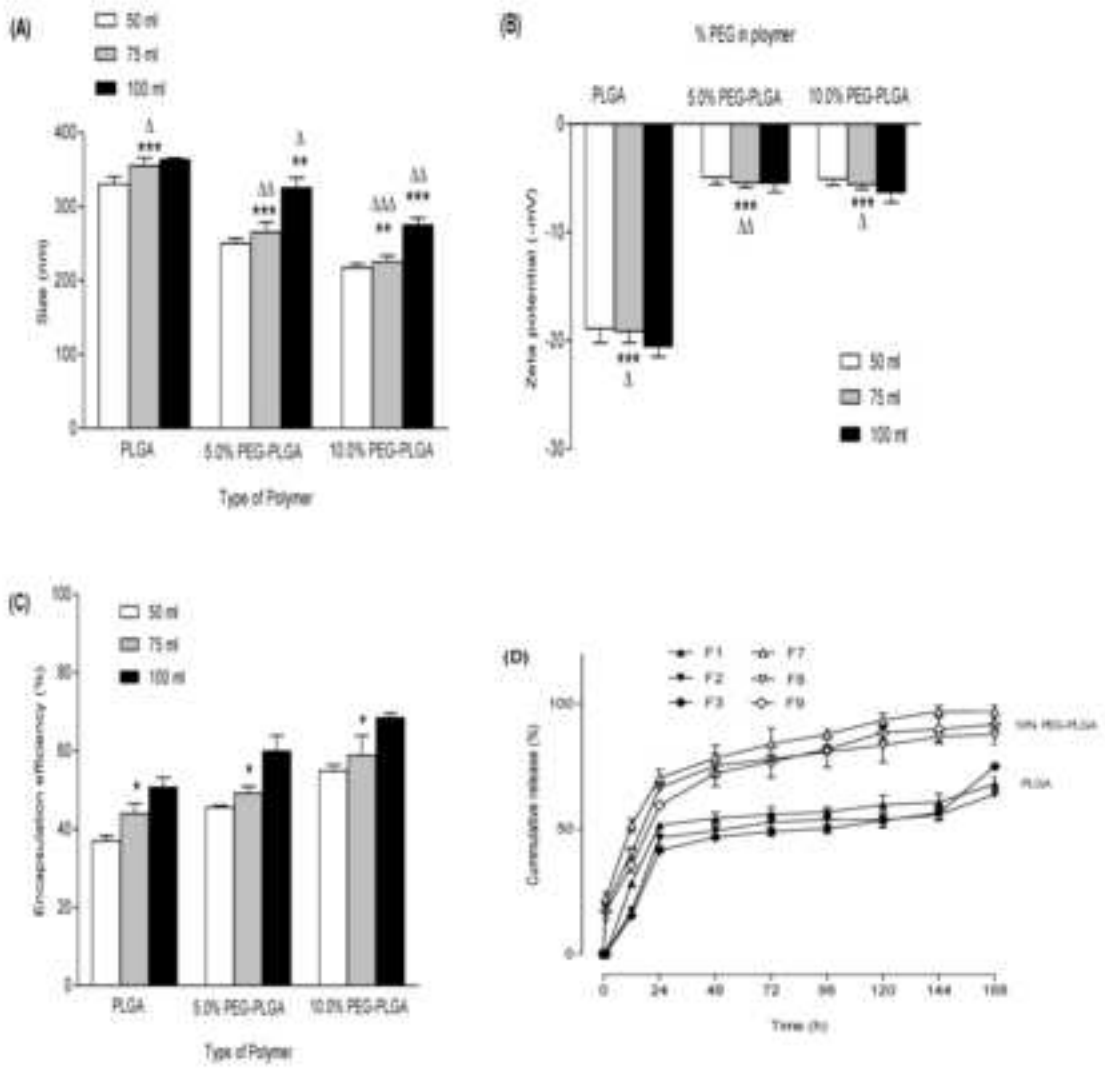

Figure 2.

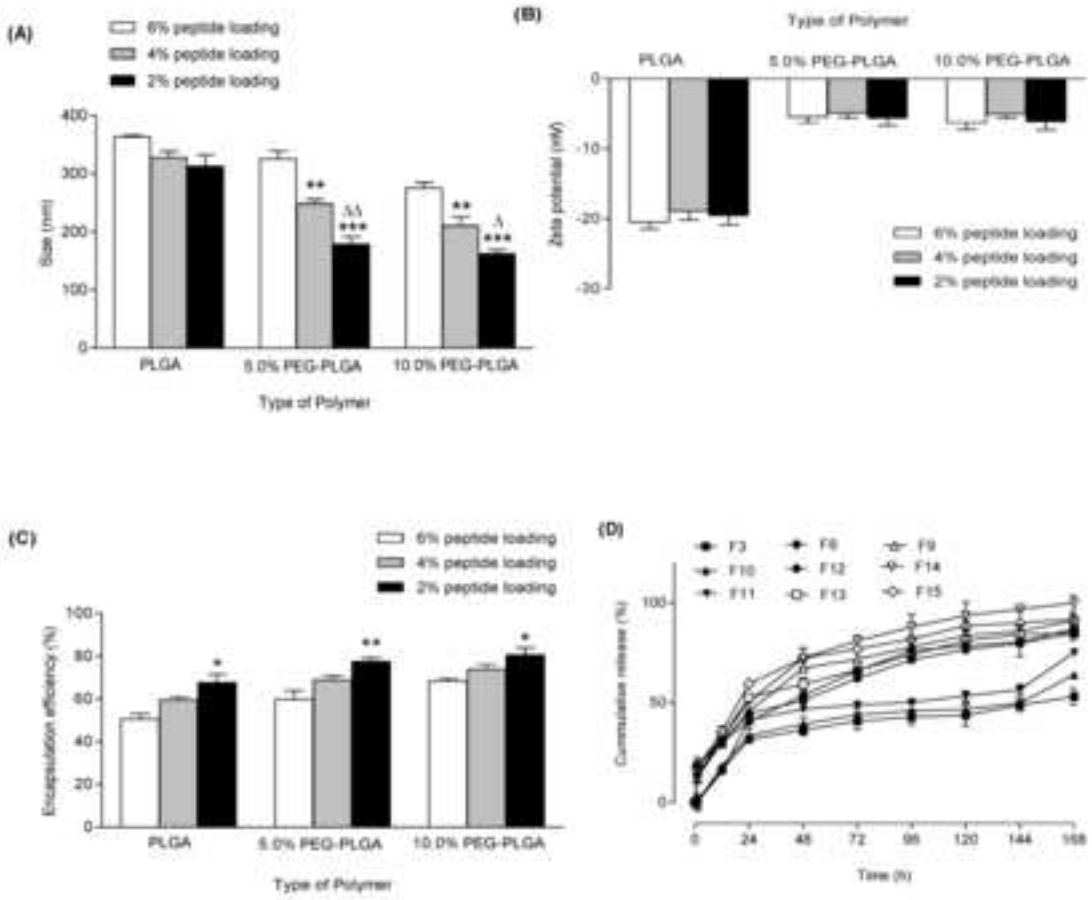
(A)
6% peptide loading
4% peptide loading
2% peptide loading
Size (nm)
PLGA
5.0% PEG-PLGA
10.0% PEG-PLGA
Type of Polymer
(B)
Type of Polymer
PLGA
5.0% PEG-PLGA
10.0% PEG-PLGA
Zeta potential (mV)
6% peptide loading
4% peptide loading
2% peptide loading
(C)
6% peptide loading
4% peptide loading
2% peptide loading
Encapsulation efficiency (%)
PLGA
5.0% PEG-PLGA
10.0% PEG-PLGA
Type of Polymer
(D)
F3
F6
F9
F10
F12
F14
F11
F13
F15
Cumulative release (%)
Time (h)

Figure 3.

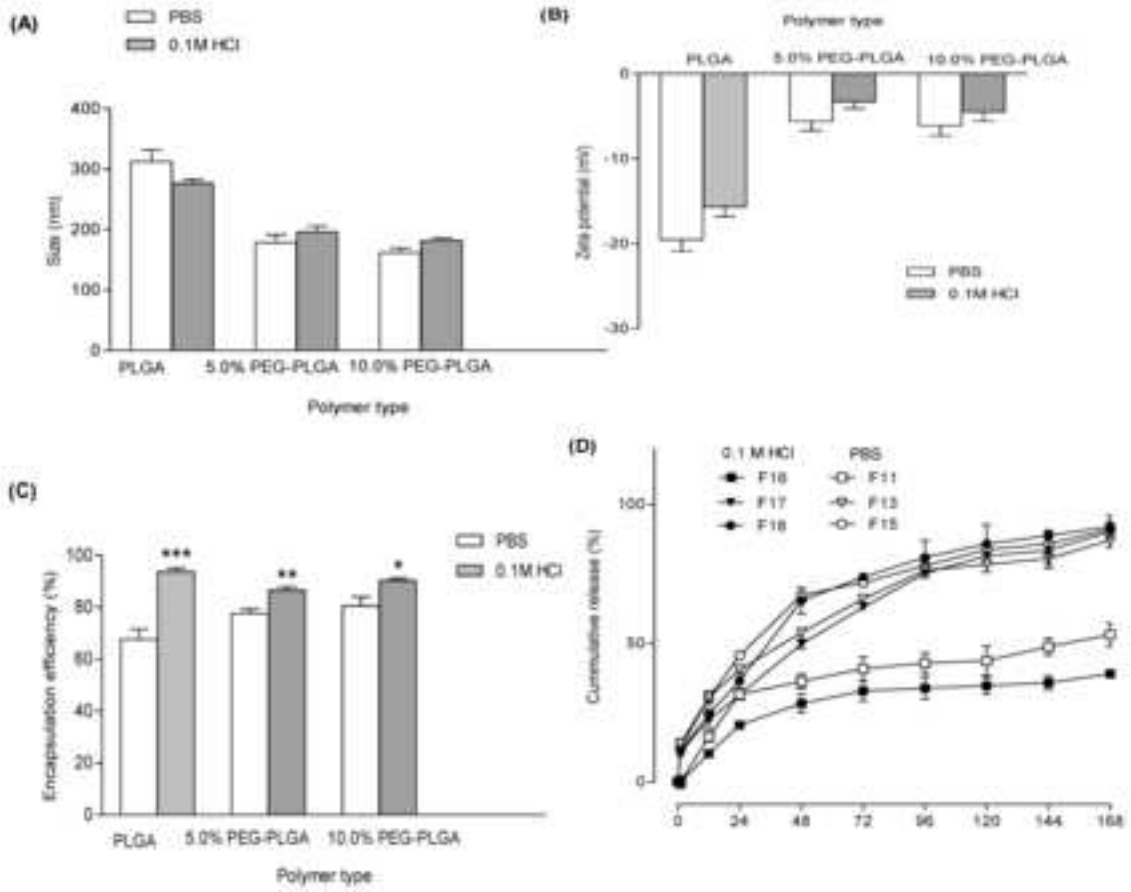
(A)
PBS
0.1M HCl
Size (nm)
400
300
200
100
0
PLGA
5.0% PEG-PLGA
10.0% PEG-PLGA
Polymer type
(B)
Polymer type
PLGA
5.0% PEG-PLGA
10.0% PEG-PLGA
Zeta potential (mV)
0
-10
-20
-30
PBS
0.1M HCl
(C)
PBS
0.1M HCl
***
**
*
Encapsulation efficiency (%)
100
80
60
40
20
0
PLGA
5.0% PEG-PLGA
10.0% PEG-PLGA
Polymer type
(D)
0.1 M HCl
F16
F17
F18
PBS
F11
F13
F15
Cumulative release (%)
100
50
0
0
24
48
72
96
120
144
168

Figure 4.

Figure 5A

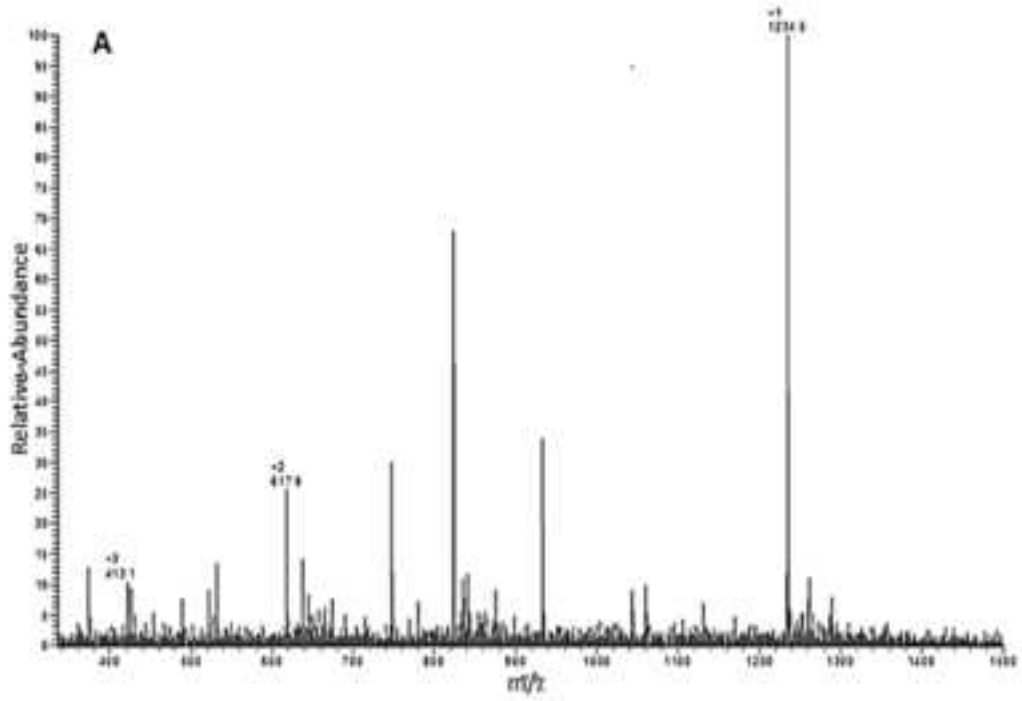

Fig. 5A

Figure 5B

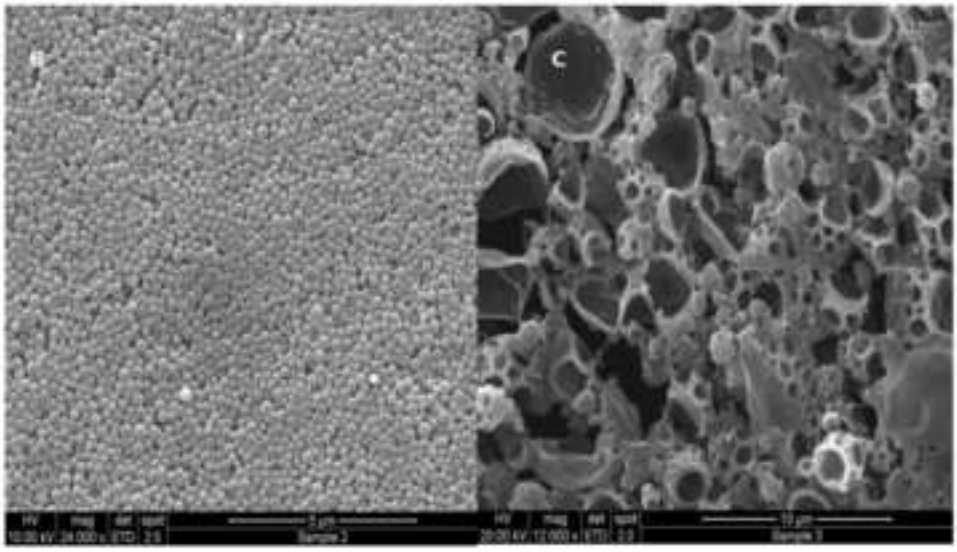

Fig. 5B and Fig. 5C

Figure 6

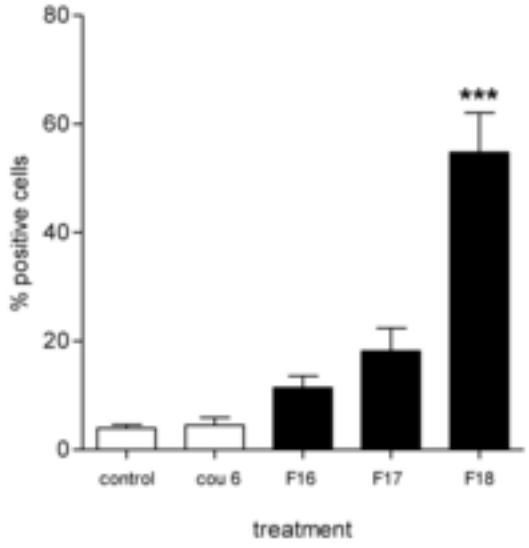

Figure 6.

Figure 7

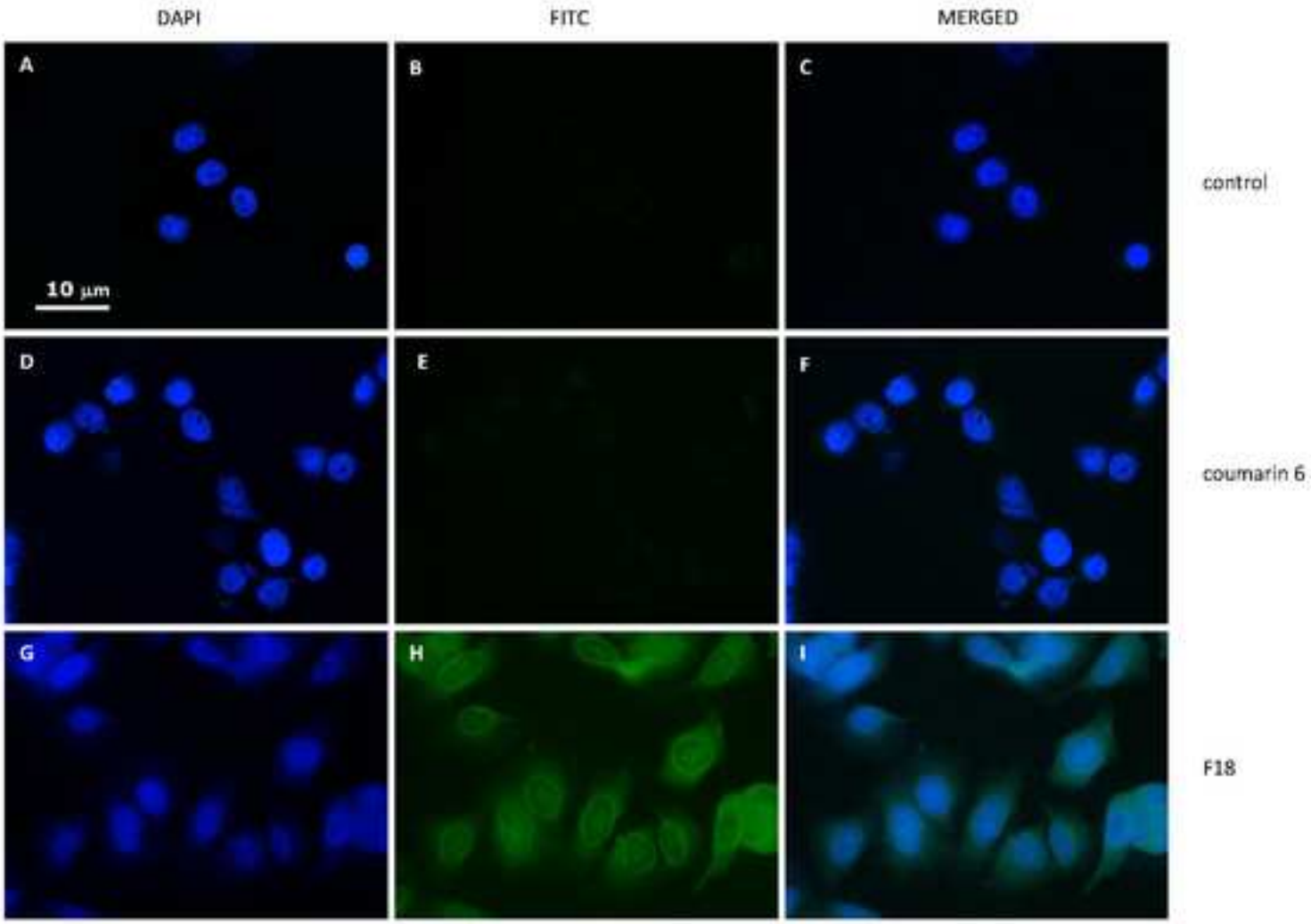

Figure 8

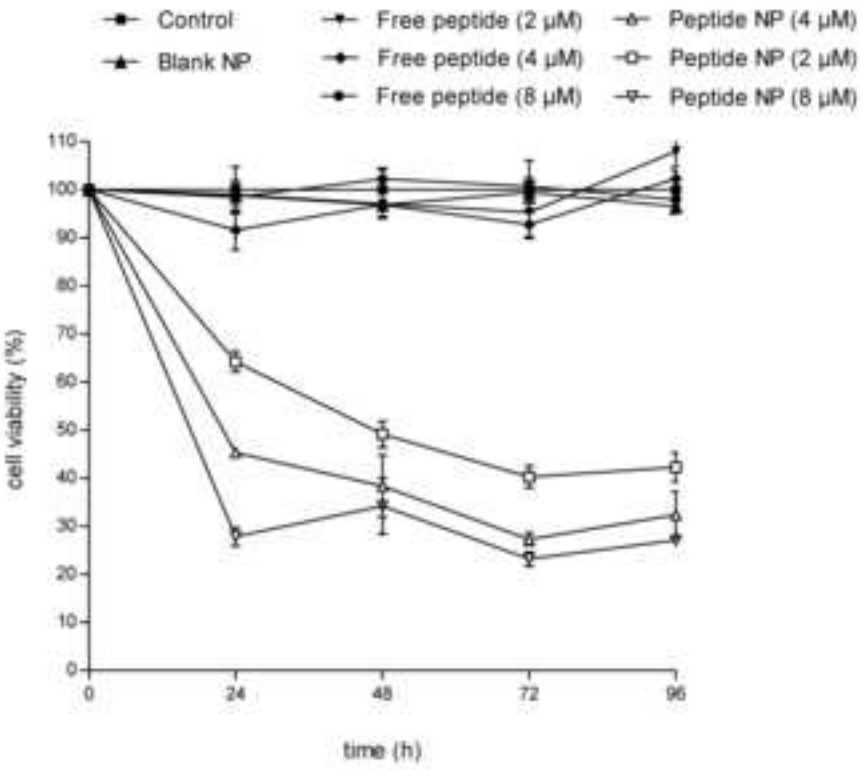

Figure 8

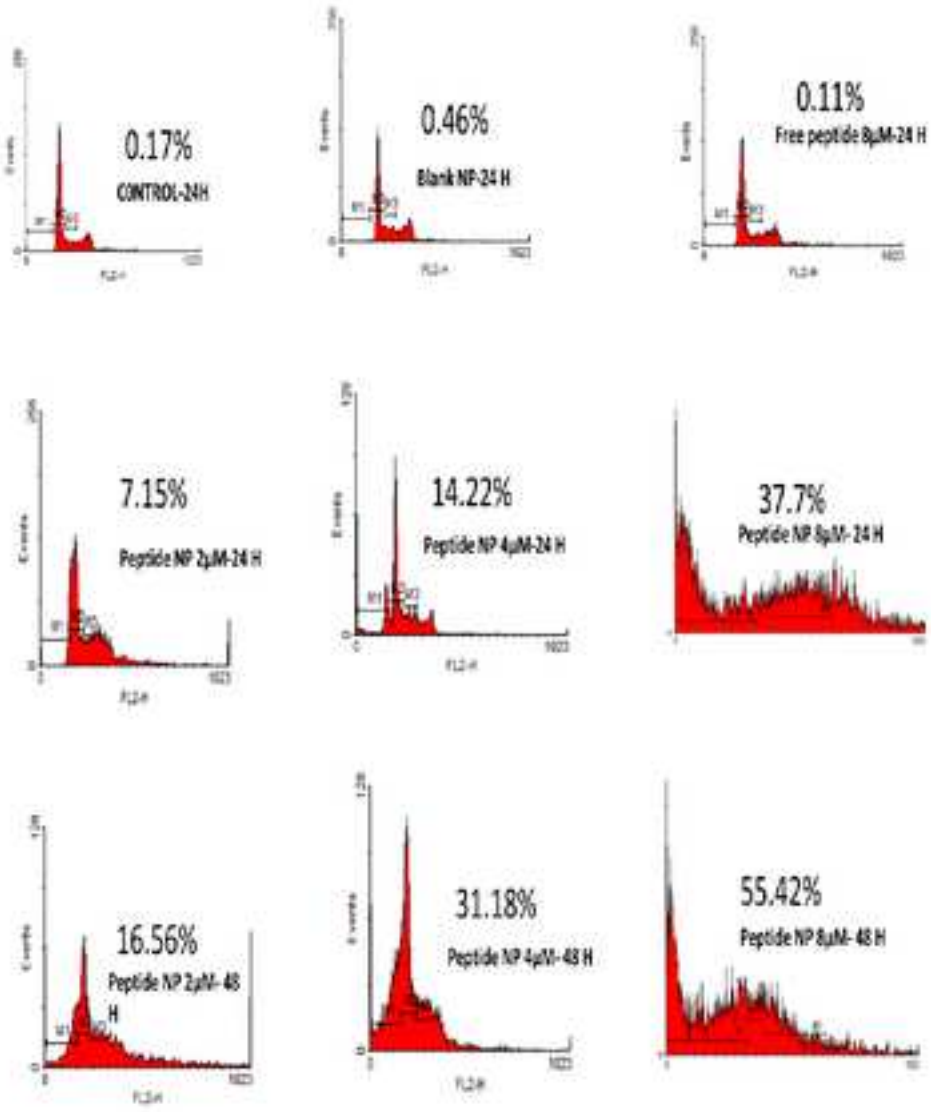
0.17%
CONTROL-24H
0.46%
Blank NP-24 H
0.11%
Free peptide 8µM-24 H
7.15%
Peptide NP 2µM-24 H
14.22%
Peptide NP 4µM-24 H
37.7%
Peptide NP 8µM- 24 H
16.56%
Peptide NP 2µM- 48 H
31.18%
Peptide NP 4µM- 48 H
55.42%
Peptide NP 8µM- 48 H

Figure 9

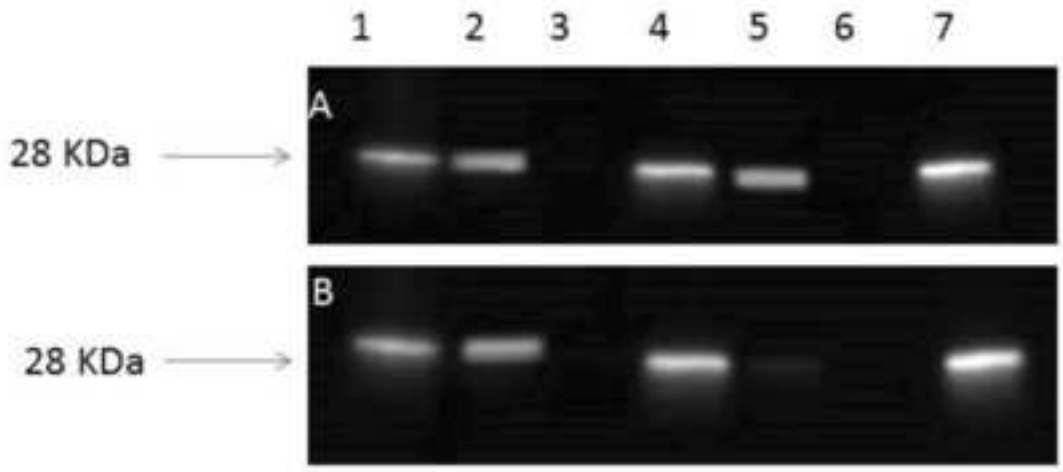

Figure 10